Ambient-Processed Colloidal Quantum Dot Solar Cells via Individual Pre-Encapsulation of Nanoparticles

Ratan Debnath,[†] Jiang Tang,[†,‡] D. Aaron Barkhouse,[†] Xihua Wang,[†]
Andras G. Pattantyus-Abraham,[†] Lukasz Brzozowski,[†] Larissa Levina,[†] and Edward H. Sargent*,[†,‡]

*Department of Electrical and Computer Engineering, University of Toronto, 10 King's College Road, Toronto,
Ontario M5S 3G4, Canada, and Department of Materials Science and Engineering, University of Toronto,
184 College Street, Toronto, Ontario M5S 3E4, Canada*

Received February 24, 2010; E-mail: ted.sargent@utoronto.ca

Solution-processed solar cells employing colloidal quantum dots (CQDs) offer the potential to produce large area, low-cost photovoltaics with improved efficiencies.[1−3] Size-effect tuning provides absorption and, prospectively, efficient conversion of the sun's full energy spectrum spanning the visible, near-IR, and short-wavelength IR. Since optimally designed single-junction and tandem solar cells both rely on IR-band-gap semiconductors, there has been much recent emphasis on this spectral region. PbS, PbSe, and $PbS_xSe_{1−x}$ CQDs featuring widely tunable size-effect band gap control have been exploited in a single, planar Schottky device architecture. Promising solar power conversion efficiencies (PCEs) of 3.3%[2] and 3.4%[4] have been reported in devices based on $PbS_xSe_{1−x}$ and PbSe CQDs, respectively.

In all reports, these devices have been found to suffer from extreme air sensitivity. Fabrication and characterization processes must be carried out in a rigorously controlled inert environment. At least two mechanisms deleterious to device performance are expected to be at work. First, these devices rely on the establishment of a depletion region in which photogenerated charge carriers are swept to their respective electrical contacts. Oxidation produces increased p-type doping, reducing the spatial extent of the depletion region and correspondingly reduced photocurrent. Second, oxidation of metal chalcogenide surfaces has been shown to produce deep traps for electrons. These may act as recombination centers[5] and also impede electron transport.[6] The resulting requirement that processing be carried out in a highly controlled environment significantly curtails the low-cost, large-area processability that is otherwise afforded by solution-processed materials systems.

Here we report a new strategy for fabricating CQD solar cells. Our approach overcomes these limitations, enabling processing in air. We showcase the utility of our new ligand strategy and obtain a 3.6% AM1.5 (solar spectrum) PCE from these devices.

Organic ligands such as oleic acid and trioctylphosphine/trioctylphosphine oxide are employed in the synthesis of highly monodispersed, well-passivated nanoparticles.[7] Because these long, insulating ligands prevent efficient charge transport within CQD solids, exchange of the capping ligands to a shorter molecule is often practiced. More weakly bound ligands such as butylamine[8] and pyridine[9] have often been employed because these facilitate subsequent further manipulations such as solid-state cross-linking or densification of films.

We hypothesized that it is the use of weakly bound ligands that is responsible for the ready access of oxygen and water to the undefended surface of CQDs. We therefore pursued the obverse of the usually practiced strategy: we sought a ligand that would be

maximally strongly bound. We selected *N*-2,4,6-trimethylphenyl-*N*-methyldithiocarbamate (TMPMDTC) because (1) it is small and conjugated, thus necessitating no substitution once the nanoparticles are incorporated into films that require electrical transport, and (2) the carbodithiolate $[−C(S)S^−]$ group is bound to the nanoparticle surface via a pair of very strong thiol-to-metal-cation bonds. We expected that these ligands would anchor strongly to the nanocrystal, readily displacing oleic acid from its surface and providing resistance to oxidative attack and even to displacement in subsequent solid-state film treatments.

We prepared TMPMDTC by combining carbon disulfide with the appropriate amines.[10] Ligand exchange was carried out at room temperature by mixing TMPMDTC with oleic acid-capped PbS CQDs. As shown in Figure 1A, the absorption spectrum of oleate-capped PbS CQDs showed a well-defined excitonic peak with a maximum at 923 nm. When these PbS CQDs were subjected to ligand exchange with TMPMDTC for 4 h, the absorption peak was blue-shifted to 880 nm and the peak width was substantially increased. The blue shift of the excitonic peak is likely due to the partial etching of PbS CQDs during ligand exchange, and the broadening of the excitonic peak is attributable to the increased nanocrystal size polydispersity, as observed upon pyridine ligand exchange of PbS nanocrystals.[11] IR spectra (Figure 1B) showed a dramatic reduction in the intensity of C−H vibrations at 2924 cm^{-1} (asymmetric) and 2854 cm^{-1} (symmetric) that are signatures of the
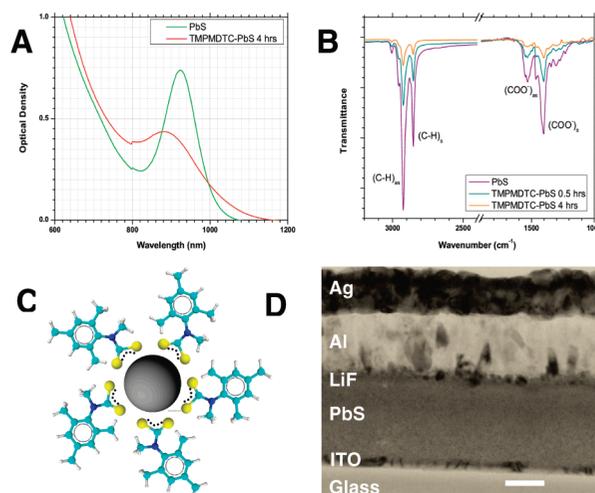
Figure 1. (A) Absorption and (B) FTIR spectra of PbS CQDs before and after TMPMDTC ligand exchange. (C) Schematic demonstration of passivation of a PbS CQD (gray sphere) by TMPMDTC ligands (yellow, sulfur; blue, nitrogen; cyan, carbon; white, hydrogen). (D) Cross-sectional TEM image of a typical device showing ITO/PbS CQD film/LiF/metal contacts. The scale bar represents 100 nm.

† Department of Electrical and Computer Engineering.
‡ Department of Materials Science and Engineering.

presence of oleic acid. Strong reduction of symmetrical and asymmetrical COO^- vibrations at 1398 and 1528 cm^{-1}, respectively, from the carboxylate group provided confirmatory evidence of substantial ligand exchange. Transmission electron microscopy (TEM) revealed a reduction in interdot spacing from 2.5 to 1 nm following exchange. Prior reports suggest that hopping dominates transport under these conditions.[6]

TMPMDTC-capped PbS CQDs (Figure 1C) were used for the fabrication of Schottky solar cells in ambient air using a layer-by-layer process.[12] PbS CQDs films were fabricated on precleaned, indium tin oxide (ITO)-coated glass substrates (Delta Technologies). A thin layer of TMPMDTC-capped PbS NCs (50 mg/mL in octane) was spin-coated at 2500 rpm for 15 s, after which 10 drops of 1% benzenethiol in acetonitrile was applied, followed by rinsing with acetonitrile and octane. This process was repeated seven times to produce a ~230 nm film; thus, each repetition generated ~33 nm of film. Before evaporation of top contacts (100 nm Al and 80 nm Ag) on the NC surface, a thin 0.8 nm LiF layer was first thermally evaporated to improve the quality of the Schottky junction between the PbS CQD film and the Al electrodes. All of the electrical contacts were deposited at 10^{-5} Torr using an Edwards Auto 306 system through a shadow mask with 1.92 mm diameter circular contacts corresponding to an active cell area of 2.9 mm^2.

Figure 1D shows a cross-section TEM characterization of our glass/ITO/PbS CQD film/LiF/Al/Ag Schottky solar cells. The PbS CQD film was dense and crack-free. We studied the net doping of our thin films using capacitance−voltage characterization. We obtained a carrier density of 4×10^{16} cm^{-3} and a depletion region thickness of ~220 nm. This represents a 3-fold decrease in doping and a 50% increase in depletion region depth relative to prior reports,[13] including those processed under an inert atmosphere. We were thus poised to achieve the high external quantum efficiencies that were the objective of this work.
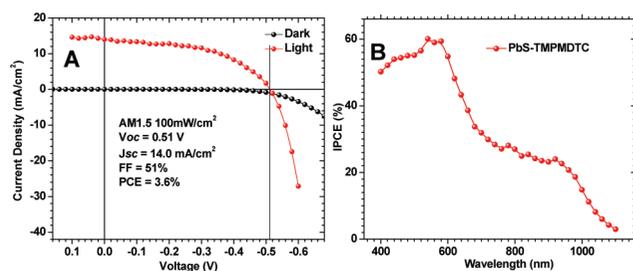
Figure 2. (A) $I-V$ characteristic and (B) IPCE spectrum of TMPMDTC−PbS CQD Schottky solar cells.

The current−voltage ($I-V$) characteristic of our best device is shown in Figure 2A. Under simulated 99.8 mW/cm^2 AM1.5G solar illumination, the device showed an open-circuit voltage (V_{oc}) of 0.51 V, a short-circuit current density (J_{sc}) of 14.0 mA/cm^2, and a fill factor (FF) of 51%, corresponding to a PCE of 3.6%. Our best FF in these Schottky devices was 60%, and our best V_{oc} was 0.54 V; the average PCE of six devices was (3.28 ± 0.24)%. Unencapsulated devices were stable operating in air for 0.5 h under continuous AM1.5 illumination and degraded in performance by ~20% after multiple hours of operation. Figure 2B shows the typical incident photon conversion efficiency (IPCE) spectrum of our device. IPCEs of ~20% at an excitonic peak wavelength of 920 nm and ~60% at 560 nm were achieved from these devices. Integration of the external quantum efficiency (EQE) spectrum with the standard ASTM G173−03 AM1.5G spectra yielded a J_{sc} value of 14.5 mA/cm^2, in excellent agreement with our measured value of 14.0 mA/cm^2.

We sought to gain further insight into the trap states and their evolution in ambient air for the case of TMPMDTC-based devices in comparison with a control. To do so, we measured the capacitance at a number of frequencies corresponding to the inverse time constants of long-lived, deep traps. We report the results in Figure 3. The control exhibited a large increase in low-frequency capacitance consistent with the emergence of deep traps likely traceable to sulfate ($PbSO_4$) formation. In contrast, the TMPMDTC device did not change significantly across the same frequency regime.
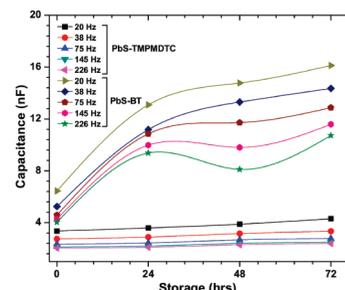
Figure 3. Capacitance plots at various low frequencies for solar cells stored in ambient air for 3 days. The PbS−TMPMDTC devices exhibited little change in capacitance and its frequency dependence, while devices without TMPMDTC (PbS−BT) showed a dramatic change.

In summary, a strongly bound, bidentate ligand, TMPMDTC, was developed to passivate PbS CQDs through a solution exchange process. This ligand reduces the air sensitivity of the materials used in processing, enabling us to produce record-efficiency solar cells using an ambient process. These findings may be of utility beyond photovoltaics, such as in CQD light-emitting diodes and photodetectors.

References

(1) Luther, J. M.; Law, M.; Beard, M. C.; Song, Q.; Reese, M. O.; Ellingson, R. J.; Nozik, A. J. *Nano Lett.* **2008**, *8*, 3488.
(2) Ma, W.; Luther, J. M.; Zheng, H. M.; Wu, Y.; Alivisatos, A. P. *Nano Lett.* **2009**, *9*, 1699.
(3) Sargent, E. H. *Adv. Mater.* **2008**, *20*, 3958.
(4) Choi, J. J.; Lim, Y. F.; Santiago-Berrios, M. B.; Oh, M.; Hyun, B. R.; Sung, L. F.; Bartnik, A. C.; Goedhart, A.; Malliaras, G. G.; Abruna, H. D.; Wise, F. W.; Hanrath, T. *Nano Lett.* **2009**, *9*, 3749.
(5) Barkhouse, D. A. R.; Pattantyus-Abraham, A. G.; Levina, L.; Sargent, E. H. *ACS Nano* **2008**, *2*, 2356.
(6) Konstantatos, G.; Levina, L.; Fischer, A.; Sargent, E. H. *Nano Lett.* **2008**, *8*, 1446.
(7) Murray, C. B.; Norris, D. J.; Bawendi, M. G. *J. Am. Chem. Soc.* **1993**, *115*, 8706.
(8) Johnston, K. W.; Pattantyus-Abraham, A. G.; Clifford, J. P.; Myrskog, S. H.; MacNeil, D. D.; Levina, L.; Sargent, E. H. *Appl. Phys. Lett.* **2008**, *92*, 151115.
(9) Gur, I.; Fromer, N. A.; Alivisatos, A. P. *Science* **2005**, *310*, 462.
(10) Querner, C.; Reiss, P.; Bleuse, J.; Pron, A. *J. Am. Chem. Soc.* **2004**, *126*, 11574.
(11) Hanrath, T.; Veldman, D.; Choi, J. J.; Christova, C. G.; Wienk, M. M.; Janssen, R. A. *ACS Appl. Mater. Interfaces* **2009**, *1*, 244.
(12) Luther, J. M.; Law, M.; Song, Q.; Perkins, C. L.; Beard, M. C.; Nozik, A. J. *ACS Nano* **2008**, *2*, 271.
(13) Johnston, K. W.; Pattantyus-Abraham, A. G.; Clifford, J. P.; Myrskog, S. H.; Hoogland, S.; Shukla, H.; Klem, E. J. D.; Sargent, E. H. *Appl. Phys. Lett.* **2008**, *92*, 122111.

JA1013695